IEEE Access
Multidisciplinary | Rapid Review | Open Access Journal

Received October 26, 2018, accepted December 11, 2018, date of publication January 9, 2019, date of current version February 6, 2019.

Digital Object Identifier 10.1109/ACCESS.2018.2889182

Effects of Elastic Hinges on Input Torque Requirements for a Motorized Indirect-Driven Flapping-Wing Compliant Transmission Mechanism

CHAO ZHANG[1,2] AND CLAUDIO ROSSI[3]

[1]Department of Automation, Shanghai Jiao Tong University, Shanghai 200240, China
[2]Key Laboratory of System Control and Information Processing, Ministry of Education, Shanghai 200240, China
[3]Centre for Automation and Robotics, UPM-CSIC, 28006 Madrid, Spain

Corresponding author: Claudio Rossi (claudio.rossi@upm.es)

The work of C. Zhang was supported by the China Scholarship Council (CSC). The work of C. Rossi was supported in part by the RoboCity2030-III-CM Project (S2013/MIT-2748, Robotica aplicada a la mejora de la calidad de vida de los ciudadanos, fase III), through the Programas de Actividades I+D en la Comunidad de Madrid, and in part by the Structural Funds of the EU.

ABSTRACT This paper presents compliant transmission mechanisms for a flapping-wing micro air vehicle. The purpose of this mechanism is to reduce power consumption, a critical issue in this kind of vehicles, as well as to minimize the peak input torque required by the driving motor, which helps to maintain flight stability and reduces mechanical shocks of the structure. We first describe the development of pseudo-rigid-body model of the mechanism and the analysis of the corresponding kinematics. Second, we compute the required input torque for driving stable flapping motions, from the perspectives of work and energy. For this computation, two methods are applied, one based on the principle of virtual work and another one based on rigid-body dynamics. Our mathematical analysis demonstrates that both methods are consistent with each other in terms of the resulting input torque from the motor. Finally, according to the results from the input torque analysis, the main parameters characterizing the compliant joints, the torsional stiffness of virtual spring and initial neutral angular position, are optimized. The experimental results carried out with two different mechanical setups, one with rigid components, and another one with flexible components, demonstrate the relationship between the input voltage (that is directly related to flapping frequency) and power saving of the compliant mechanism. The average power consumption is reduced of up to 4%, and peak power consumption is reduced up to 25% using the compliant transmission mechanisms compared to the rigid mechanism. The experiments also show a clear relationship between flapping frequency and power savings.

INDEX TERMS Compliant transmission mechanisms, compliant structures, virtual work, flapping-wing micro air vehicles, FWMAVs.

I. INTRODUCTION

Micro Aerial Vehicles (MAVs) are unmanned aerial vehicles whose size is of the order of few centimeters of wingspan and mass less than few hundred grams. Thanks to their small size and high maneuverability, MAVs are ideal for many applications such as reconnaissance in confined spaces, search and rescue, or hazardous environment exploration. Because of their size, however, the design of MAVs implies important technological challenges, such as low power consumption. FWMAVs adopt flapping wings for generating lift forces, but also for maneuvering. Many researchers in this field have looked into the biological world in an attempt to understand the keys of efficient flight, especially, for scale reasons, concentrating on insects [5], [6], [11], [29].

Here, we focus on flapping. Entomology studies demonstrated that insects can decrease the power consumption by storing and releasing elastic energy in the elements [10], [26], [27] of their musculoskeletal flapping system, concretely the thorax (tergal plate) [22], flight muscles [1] and wing hinges [4] (see Fig. 1). Moreover, it has been pointed out

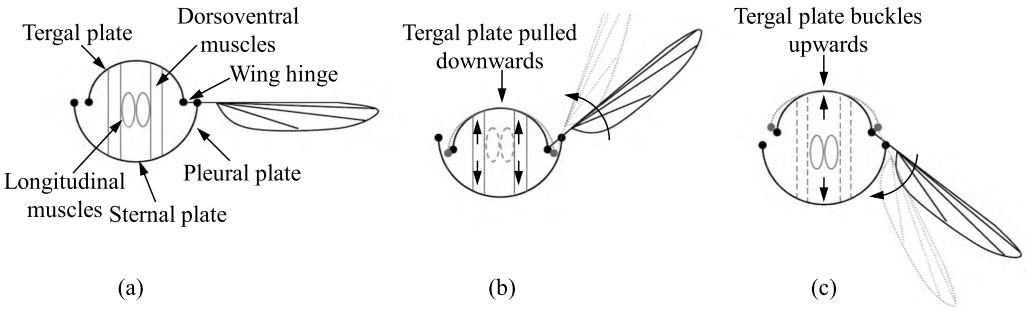

FIGURE 1. Schematic drawing of insect thorax: (a) basic anatomy; (b) upstroke; (c) downstroke.

by anonymous reviewers that compliant connectivity is likely a ubiquitous feature of flight systems in general, including both insect and vertebrate flyers. Compliant flapping mechanisms, therefore, could also be applied to bird-size FWMAVs, that mostly adopt traditional rigid-body mechanisms because they have high forces and energy conversion efficiency [19].

The mechanism works as follows: at the end of each wing stroke (upstroke or downstroke), the kinetic energy of the wings is transformed into elastic energy in the compliant elements of the thorax mentioned above. This has a twofold effect: at the end of a stroke, it helps decelerating the wings and reduces the sharp shock when the wing changes direction. The latter feature is particularly interesting as in principle it allows building lighter structures (therefore saving weight at the benefit of available payload and/or mission autonomy) and helps flight stability. Then, at the beginning of the next wing stroke, the energy stored is released, helping accelerating the wings.

Therefore, we took such feature as a model to imitate in order to construct our flapping-wing aerial vehicle.

A. RELATED WORK

Attempts to imitate insects' energy-saving capabilities can be found in the literature. Coil springs are usually incorporated as elastic elements into the flapping-wing mechanisms. Research results from both Madangopal *et al.* [16] and Baek *et al.* [3] show that the introduction of linear coil springs can minimize the required input peak torque or input power. The use of linear coil springs which are directly connected to DC motors in direct-driving flapping-flight prototypes can also be found in the literature [2], [12]. However, additional springs bring additional weight and have no effect in reducing joint friction energy losses [15].

Piezoelectric actuators are also used to fabricate the flapping transmissions due to their capability of high power densities and high efficiencies [12], [30]. Generally, piezoelectric actuators driving transmissions are designed to operate at their resonance frequency and are also used as active springs coupled with the mechanisms for storing energy [21], [29]. One flying prototype driven by piezoelectric actuators capable of liftoff and stable hovering has been presented in [24]. One drawback of piezoelectric actuators is that they are not suitable for systems with a high desired payload due to their high power requirements and limits in displacement and forces [12]. Recently, electromagnetic actuators, similar to piezoelectric actuators, were also introduced to couple with the mechanism for driving flapping wings toward resonance [6], [17], [18].

Compared to spring mechanisms and piezoelectric or electromagnetic actuators, compliant mechanisms are attractive solutions. Such mechanisms are multifunctional structures which combine functions of mechanical parts with elastic energy-stored components together [23]. These characteristics allow reproducing insects' energy-saving capabilities. Moreover, compared to rigid-body mechanisms, compliant mechanisms have lower wear, friction, and backlash [8], [28].

Additionally, they reduce the peak input torque and sharp shocks of the mechanism, which has direct benefits in allowing lighter structures and smaller batteries, at the benefit of the payload and/or flight time.

Some examples of compliant mechanisms for FWMAVs can be found in the literature. In [7], a thorax-like clicking compliant mechanism inspired by an insect named *Dipteran* is proposed. This research showed that clicking compliant mechanisms could produce more thrust per input power than a conventional rigid-body counterpart. Sahai *et al.* [20] demonstrated that flapping transmission with rubber flexural hinges can reduce input power up to 20%. For a review of compliant flapping mechanisms, readers can refer to [32].

In the literature, few works on compliant mechanisms carry out a mathematical analysis of the influences of the characteristics of compliant joints or hinges (like the stiffnesses of virtual spring and the neutral angular positions) on the final input peak torque or input power required. In [33], we presented a theoretical analysis on the transmission mechanism and the effects of the compliant attributes on the final peak input torque by using the principle of *virtual work*. We also showed how to optimise the values of the main parameters of the compliant joints, in terms of the torsional stiffness of virtual spring and initial neutral angular position, so as to minimize the peak input torque. The theoretical analysis carried out proved that using compliant transmission mechanisms could save energy up to 70% in ideal conditions.

In the following sections, we first presents the compliant transmission mechanism for a FWMAV. We then summarize the analysis of its kinematics, the aerodynamic modelling and the virtual work-based methodology for calculating the input torque from motor, result of previous work. Then, we present a comparison between two methodologies based on virtual work and rigid-body dynamics to calculate the required input torque from motor. These treat the problem from the perspectives of work and energy, but yield the same results.

Section IV describes the experiments carried out using prototypes with compliant and rigid-body mechanisms. The results of the tests show how compliant mechanisms are actually affective in reducing power consumption and peak torques during flapping. Finally, Section V concludes the paper.

II. A FLAPPING TRANSMISSION MECHANISM WITH COMPLIANT JOINTS

In this section, we present a flapping transmission mechanism with small-length lightweight compliant hinges for the bird-size FWMAV shown in Fig. 2.

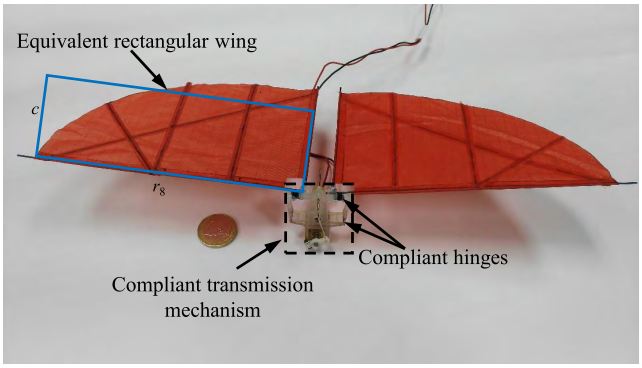

FIGURE 2. Physical prototype of the proposed flapping wing micro aerial vehicle.

A. KINEMATICS

Figure 3 (left) shows a sketch of the mechanism. The compliant hinges are modeled as revolute joints with virtual springs, as proposed in [13]. These can be seen in Fig. 3 (right). A DC motor is employed to drive the compliant transmission mechanism to realize flapping motions. The mass of wing frames is assumed to be uniformly distributed along the length of the wing spar. Table 1 reports the dimensions of the prototype.

Considering the vector loops O-A-B-C-D-O and O-A-B-O shown in Fig. 3 (right), the loop closure equations in form of complex members are:

$$r_1 e^{j\theta_1} + r_2 e^{j\theta_2} - r_3 e^{j(\pi+\theta_3)} - r_4 e^{j\theta_4} - r_6 e^{j0} - r_7 e^{j\frac{\pi}{2}} = 0 \quad (1)$$

$$r_1 e^{j\theta_1} + r_2 e^{j\theta_2} - r_5 e^{j\frac{\pi}{2}} = 0 \quad (2)$$

where r_i $(i = 1, 2, ..., 6, 7)$ are lengths of links and θ_j $(j = 1, 2, ..., 4)$ are angular positions of the corresponding links.

TABLE 1. Dimensions of the components for the compliant transmission mechanism.

Link	Symbol	Lenght
OA	r_1	6.0mm
AB	r_2	32.8mm
BC	r_3	15.0mm
CD	r_4	22.4mm
OB	r_5	—
Horizontal Distance OD	r_6	15.0mm
Vertical Distance OD	r_7	13.0mm
CE	r_8	235.0mm

The transmission mechanism has only one degree of freedom, the angular position of the crank θ_1. The rest angular positions $\theta_2, \theta_3, \theta_4$ can be treated as functions in terms of θ_1.

Given their initial values, the values of θ_1, θ_2, θ_3, θ_4 during a whole flapping cycle can be obtained from equations (1) and (2). Similarly, angular velocities $\dot{\theta}_i$ and ω_i and accelerations α_i $(i = 2, 3, 4)$ of the links can be computed according to the first and second order derivatives of the two mentioned equations.

B. AERODYNAMIC TORQUE

Aerodynamic torques generated by flapping wings play a very important role in the stable flight of FWMAVs. The aerodynamic torque produced by wing motions in a cycle were analyzed using an aerodynamic model based on the blade element theory [9]. For simplifying the calculation, the irregular shape of a wing was approximated with a rectangle, whose length and width equal the length of the wing spar r_8 and the average wing chord c, respectively (see Fig. 2). The wing is assumed to be rigid, i.e., without any twist and bend along the wing chord and the leading edge. Also, the mass of the wing is considered to be negligible. Therefore, the normal force produced by a single blade can be expressed according to the blade element theory as follows:

$$dF_a = -\frac{1}{2}\rho C_1 |V(r,t)|^2 sgn(V(r,t)) c dr, \quad (3)$$

where $V(r,t)$ is a absolute velocity of an element, whose direction is contrary to the motion of the wing, ρ is the air density, and C_1 is the normal force coefficient of the blade [14]. $V(r,t)$ consists of two parts: the translational velocity $V(r,t)_T$ and the rotational velocity of the wings $V(r,t)_R$. Since the value of the translation velocity $V(r,t)_T$ is relatively small, its effect of wings' movements is also small. Therefore, $V(r,t)$ and $V(r,t)_R$ can be considered equal i.e., $V(r,t) = V(r,t)_R$, and $V(r,t)_T$ could be simplified in the equations. In the following, the term is maintained for completeness.

The instantaneous aerodynamic torque $d\tau_a$ can be expressed by the instantaneous force dF_a times the distance r along the wing spar,

$$d\tau_a = -\frac{1}{2}\rho C_1 r^3 \omega_3^2 sgn(\omega_3) c dr \quad (4)$$

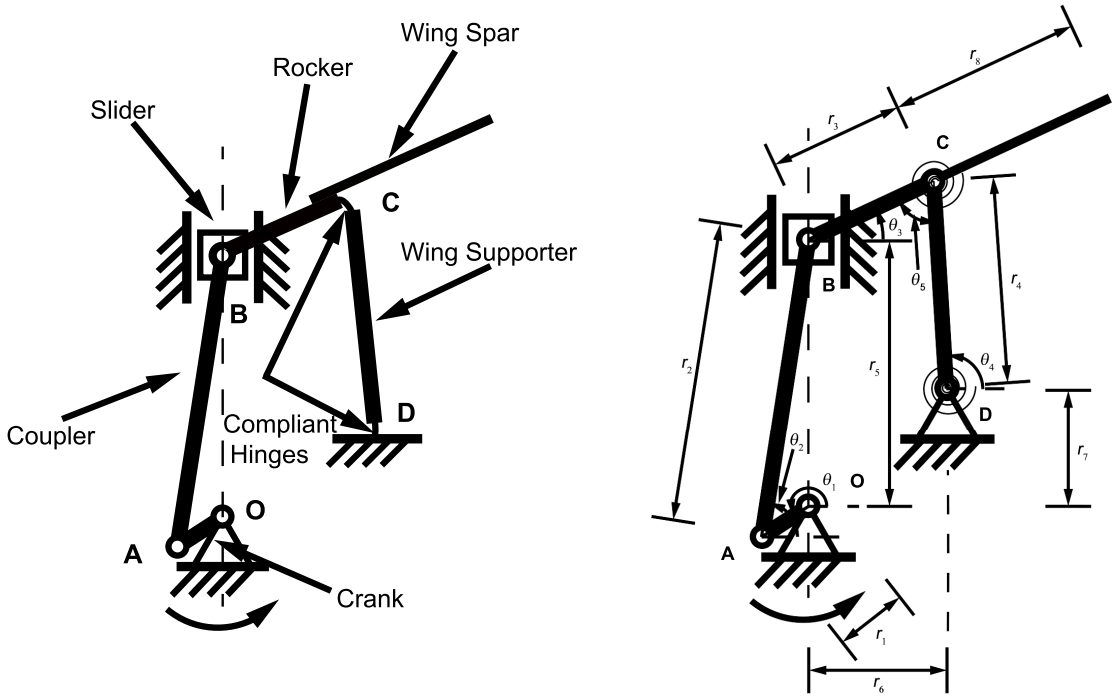

FIGURE 3. Left: Schematic view of the compliant transmission mechanism for flapping. Right: The corresponding pseudo-rigid-body model of the mechanism.

where ω_3 is the angular velocity of the rocker which wing spar. For further details see also the Appendix.

III. INPUT TORQUE CALCULATION

The input torque τ_m can be computed either with the principle of virtual work or using rigid body dynamics. In the following, we present the calculation based on both methods, and demonstrate that the same results are achieved.

A. INPUT TORQUE CALCULATION BASED ON THE PRINCIPLE OF VIRTUAL WORK

The method of virtual work is well suitable for pseudo-rigid-body models since it treats the system as a whole, and internal interaction forces are not needed to be considered. Furthermore, elastic potential energies stored in the compliant joints can be easily taken into account. Here, the masses of links (except the wing spar), inertial forces and frictions at joints are negligible in comparison with external aerodynamic forces and applied torque from the motor.

According to the PRB model shown in the Fig. 3 (right), the generalized coordinate is chosen to be the angular displacement of the crank θ_1 and its virtual displacement is $\delta\theta_1$. The total virtual work δW includes three parts: the work done by the motor through external input torque τ_m, δW_m, the work caused by inertial and aerodynamic torques of the wing, δW_w, and the work stored by the equivalent springs at compliant joints, δW_s. Thus,

$$\delta W = \delta W_m - \delta W_{inert} - \delta W_a - \delta W_s \tag{5}$$

Since the mass of wing membrane is relatively small, the mass of wing approximately equals the mass of the wing spar. As shown in the Fig. 3 (right), the motion of wing spar can be treated as a synthesis of an axis-fixed rotational movement around the joint C and a translational movement around the joint D. Therefore, the virtual work produced by the inertial torque of the rectangular wing is simply given as

$$\delta W_{inert} = \frac{1}{3} m_8 r_8^2 \alpha_3 \delta\theta_3 + m_8 r_4^2 \alpha_4 \delta\theta_4 \tag{6}$$

where m_8 is the mass of the wing spar. $\frac{1}{3} m_8\ r_8^2$ and $m_8\ r_4^2$ are the inertias of the wing with respect to the joint C and D, respectively. In addition, the virtual work δW_a caused by aerodynamic forces is given as $\delta W_a = -\tau_a \delta\theta_3$, therefore,

$$\delta W_w = \frac{1}{3} m_8 r_8^2 \alpha_3 \delta\theta_3 + m_8 r_4^2 \alpha_4 \delta\theta_4 - \tau_a \delta\theta_3 \tag{7}$$

The virtual work at compliant joints is $\delta W_s = -\sum_{i=1}^{2} Ts_i \delta\psi_i$, where $Ts_i = -Ks_i \psi_i, (i = 1, 2)$, Ks_i is the torsional stiffness constant at the ith $(i = 1, 2)$ compliant joint. Note that that joints C, D are defined as the 1st and 2nd joints, respectively. ψ_i is the angular variation at the ith joint, which is expressed as $\psi_1 = \theta_4 - \theta_{4,0}$, $\psi_2 = \theta_5 - \theta_{5,0}$ and those associated with $\delta\psi_i$ are: $\delta\psi_1 = \delta\theta_4$, $\delta\psi_2 = \delta\theta_5$. Here, θ_j, $\theta_{j,0}$ $(j = 4, 5)$ are the angular position and neutral angular position at the two compliant joints, respectively. Be ware that $\theta_5 = \theta_4 - \theta_3$, $\theta_{5,0} = \theta_{4,0} - \theta_{3,0}$, therefore, $\delta\theta_5 = \delta\theta_4 - \delta\theta_3$, $\delta\psi_2 = \delta\theta_5 = \delta\theta_4 - \delta\theta_3$. The total virtual work stored in the

two compliant joints is

$$\delta W_s = Ks_1(\theta_4 - \theta_{40})\delta\theta_4 + Ks_2[(\theta_4 - \theta_3) - (\theta_{4,0} - \theta_{3,0})](\delta\theta_4 - \delta\theta_3) \quad (8)$$

According to the principle of the virtual work, the total virtual work is set to equal to zero. The Eq. (5) can be solved in terms of the unknown input torque τ_m as,

$$\tau_m = \frac{1}{3}m_8 r_8^2\alpha_3\dot{\theta}_3 + m_8 r_4^2\alpha_4\dot{\theta}_4 - \tau_a\dot{\theta}_3 + Ks_1(\theta_4 - \theta_{40})\dot{\theta}_4 + Ks_2[(\theta_4 - \theta_3) - (\theta_{4,0} - \theta_{3,0})](\dot{\theta}_4 - \dot{\theta}_3) \quad (9)$$

B. INPUT TORQUE CALCULATION BASED ON RIGID-BODY DYNAMICS

In the previous section, we have already calculated the input torque needed based on the principle of virtue work. In this section, we solve the same problem from a perspective of energy. First of all, we will focus on kinetic and potential energies of the mechanism. Based on the energy equations, a rigid-body dynamic model is built for clearly understanding the requirement for input torque from the motor during a cycle.

For the crank, it rotates around a fixed end O with a constant speed, so it only has a rotational kinetic energy, which is given as

$$\mathrm{KE}_1 = \frac{1}{2}J_1\omega_1^2 \quad (10)$$

where J_1 is its moment of inertia about the end O. As for the coupler and rocker, they possess both translational and rotational movements around their centres of mass (CoMs), therefore, their corresponding kinetic energies (KE_i) consist of two parts, i.e., translational kinematic energy (KE_{T_i}) and rotational one (KE_{R_i}),

$$\mathrm{KE}_i = \mathrm{KE}_{T_i} + \mathrm{KE}_{R_i} \quad (11)$$

in which

$$\mathrm{KE}_{Ti} = \frac{1}{2}m_i V_{ci}^2, \quad \mathrm{KE}_{Ri} = \frac{1}{2}J_i\omega_i^2, \quad (12)$$

where m_i ($i = 2, 3$) is the mass of link r_i ($i = 2, 3$), V_{ci} ($i = 2, 3$) is the absolute velocity at the CoM, J_i ($i = 2, 3$) is the moment of inertia about the corresponding CoM. Similarly, we can also calculate translational and rotational kinetic energies of the wing spar:

$$\mathrm{KE}_{T8} = \frac{1}{2}m_8 V_C^2, \quad \mathrm{KE}_{R8} = \frac{1}{2}J_8\omega_3^2 \quad (13)$$

where m_8 is the mass of link r_8, V_C is the absolute velocity at joint C, where $V_C = r_4\omega_4$, J_8 is the moment of inertia about the joint C and ω_3 is the corresponding angular velocity of the rocker which wing spar connects to.

As for the compliant wing supporter, its equivalent kinetic energy is given as follows according to the method proposed in [31],

$$\mathrm{KE}_4 = \frac{1}{8}m_4 r_4^2\omega_4^2 + \frac{1}{2}J_4\omega_4^2 \quad (14)$$

where m_4 is the mass of wing supporter r_4, V_C is the absolute velocity at joint C and J_4 is the moment of inertia around joint D.

We assumed that the robot is fixed horizontally on the earth. In this case, no potential energy is produced by gravity. The whole potential energy only contains potential parts stored by torsional springs. The stored energy in each spring can be written as,

$$P_i = -\frac{1}{2}Ks_i{\psi_i}^2 \quad (15)$$

where Ks_i and ψ_i are the same as defined in aforementioned section.

Therefore, the total kinetic and potential energies, i.e., K and P for the entire system are

$$\mathrm{KE} = \sum \mathrm{KE}_i, \quad P = \sum P_i \quad (16)$$

and then the Lagrange's equation of the whole system is

$$L = \mathrm{KE} - P \quad (17)$$

As stated above, this system has only one degree of freedom θ_1. Hence, the Lagrange's equation of motion with respect to θ_1 is

$$\frac{\mathrm{d}}{\mathrm{d}t}\left[\frac{\partial L}{\partial\omega_1}\right] - \frac{\partial L}{\partial\theta_1} = \tau_s \quad (18)$$

where τ_s is the input torque from motor with the effect of inertial moments of links and torsional springs.

Suppose that the mass of link r_i ($i = 1, 2, 3, 4$) is too small to be ignored, therefore, $\mathrm{KE}_i = 0$ ($i = 1, 2, 3, 4$). In such case, the Lagrange's equation is

$$L = \frac{1}{2}m_8 V_C^2 + \frac{1}{2}J_8\omega_3^2 + \frac{1}{2}Ks_1{\psi_1}^2 + \frac{1}{2}Ks_2{\psi_2}^2 \quad (19)$$

Substituting Eq. (19) into Eq. (18), we can obtain

$$\tau_s = \frac{1}{3}m_8 r_8^2\alpha_3\dot{\theta}_3 + m_8 r_4^2\alpha_4\dot{\theta}_4 + Ks_1(\theta_4 - \theta_{40})\dot{\theta}_4 + Ks_2[(\theta_4 - \theta_3) - (\theta_{4,0} - \theta_{3,0})](\dot{\theta}_4 - \dot{\theta}_3) \quad (20)$$

In order to calculate the required torque input by the DC motor, the torque generated by aerodynamic force needs to be transferred to the rotation base of the crank connecting to the motor. The equivalent aerodynamic torque produced by flapping wing is given in following equation according to [16],

$$(\tau_a)_e = -\frac{\omega_3}{\omega_1}\tau_a = -\dot{\theta}_3\tau_a \quad (21)$$

To keep a FWMAV flying stably, the motor has to overcome the torques generated by compliant joints and aerodynamic forces. Therefore, the total required input torque from the motor is

$$\tau_m = \tau_s + (\tau_a)_e \quad (22)$$

Substituting Eqs. (20) and (21) into Eq. (22), then we obtain,

$$\tau_m = \frac{1}{3}m_8 r_8^2\alpha_3\dot{\theta}_3 + m_8 r_4^2\alpha_4\dot{\theta}_4 - \tau_a\dot{\theta}_3 + Ks_1(\theta_4 - \theta_{40})\dot{\theta}_4 + Ks_2[(\theta_4 - \theta_3) - (\theta_{4,0} - \theta_{3,0})](\dot{\theta}_4 - \dot{\theta}_3) \quad (23)$$

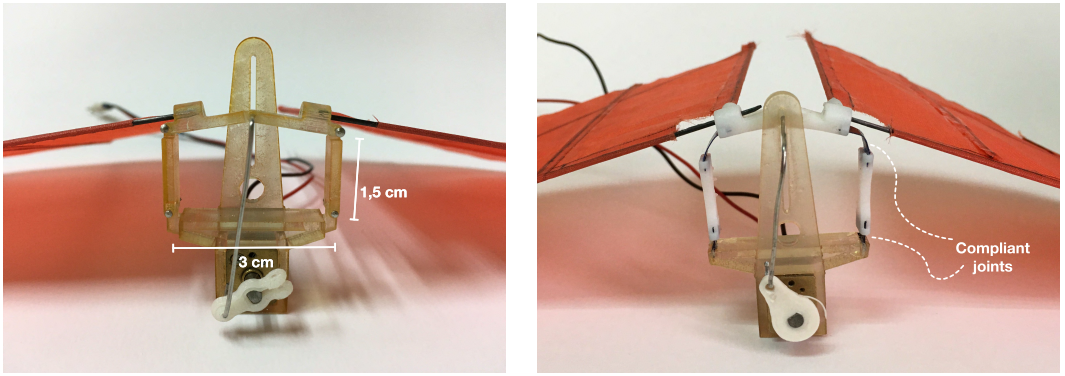

FIGURE 4. The prototypes of flapping mechanism designed. Left: rigid mechanism; Right: compliant mechanism.

Comparing Eq. (9) with Eq. (23), it can be easily notice that they actually are the same equation. This demonstrates that, for the case at hand, the method based on virtual work is as effective as the one based on classical rigid-body dynamics.

C. OPTIMIZATION

Equations (9) and (23) tell how the the torsional stiffness of the virtual spring at the compliant joint Ks_i $(i = 1, 2)$ and neutral angular position $\theta_{j,0}$ $(j = 3, 4)$ influence the input torque from the motor. For the purpose of minimizing the torque required, the optimization of Ks_1, Ks_2, $\theta_{3,0}$ and $\theta_{4,0}$ is key. Since our aim is also to minimize the peak torques $\tau_{m_{max}}$ and $\tau_{m_{min}}$, the following objective function shall be optimized:

$$F_{obj} = min(\tau_{m_{max}} - \tau_{m_{min}}) \tag{24}$$

The optimization of F_{obj}, performed in [33] using a hybrid multi-swarm particle swarm optimization algorithm [25], shown that optimal values of Ks_1 and Ks_2 are in the range of $0.8 - 1.0$, $\theta_{3,0}$ between 10 and 12 degrees and $\theta_{4,0}$ around 90 degrees. Such values provide, theoretically, a reduction of the maximum input torque between 40% and 66%, and a reduction of over 70% of the minimum torque with respect to the rigid flapping mechanism.

IV. EXPERIMENTS

In order to assess the simulation results described in the previous section, we manufactured two prototypes, one with a rigid flapping mechanism, and the other with flexible hinges (see Fig. 4).

A. MATERIALS AND METHODS

The rigid-body and compliant transmission mechanisms main parts are fabricated by a stereolithography 3D printer. All rigid mechanical elements are made of resin with tensile strength at yield of 65 MPa, and Young's modulus of 2.8 GPa. The compliant hinges are made of flexible polyvinyl chloride (PVC) with a Young's modulus of 2.8 GPa and 0.5 mm thickness.

Hinges C and D can be treated as a flexural pivots as their length is far smaller than the length of the beams that connect to them (22.4 mm and 15.0 mm). Their rotational stiffnesses of the compliant hinges can be therefore calculated according to [13]:

$$Ks_1 = \frac{E_1 \cdot I_1}{l_1} = 0.029$$

and

$$Ks_2 = \frac{E_2 \cdot I_2}{l_2} = 0.146$$

where $E_1 = E_2$ are the Young's elastic modula of the material used (2.8 GPa), $l_1 = 1$ mm and $l_2 = 5$ mm are the lengths of flexible hinges and $I_1 = I_2$ are the cross-sectional moment of inertia of the hinge, with rectangular section of height $h = 0.5$ mm and base $b = 6$ mm:

$$I_{1,2} = \frac{b * h^3}{12} = 6.25 \cdot 10^{-14} m^4$$

The two mechanisms are tested with input voltages ranging from 0 to 4.5 Volts. However, for voltages smaller than 1.5 Volts the DC motor's torque was not able to break the mechanisms' inertia and therefore no flapping took place. Hence, the actual meaningful experiments range is from 1.5 to 4.5 Volts, corresponding to flapping frequencies of approximately 3 to 9 Hz.

In order to calculate power consumption voltage and current flow were measured during flapping. For the purpose of data acquisition and control during the experiments, National Instrument Compact Rio real-time acquisition and control system has been used. Analog signals were acquired using a NI 9215 AI Module (16-Bits A/D, 100 kS/s/ch, 4- Ch). Digital control signals were generated via both a NI 9381 DIO C Series Module.

Raw signals where digitally filtered using an IIR (Infinite Impulse Response) low-pass filter in order to remove measurement noise, shown in the equation below:

$$y_n = (1 - \beta) \cdot y_{n-1} + \beta \cdot x_n \tag{25}$$

where y_n is the filtered value of sample n and x_n is the original value. The parameters adopted for the filter, according to the literature are:

$$\beta = 1 - e^{-2\pi f_c / f_s} = 0.043$$

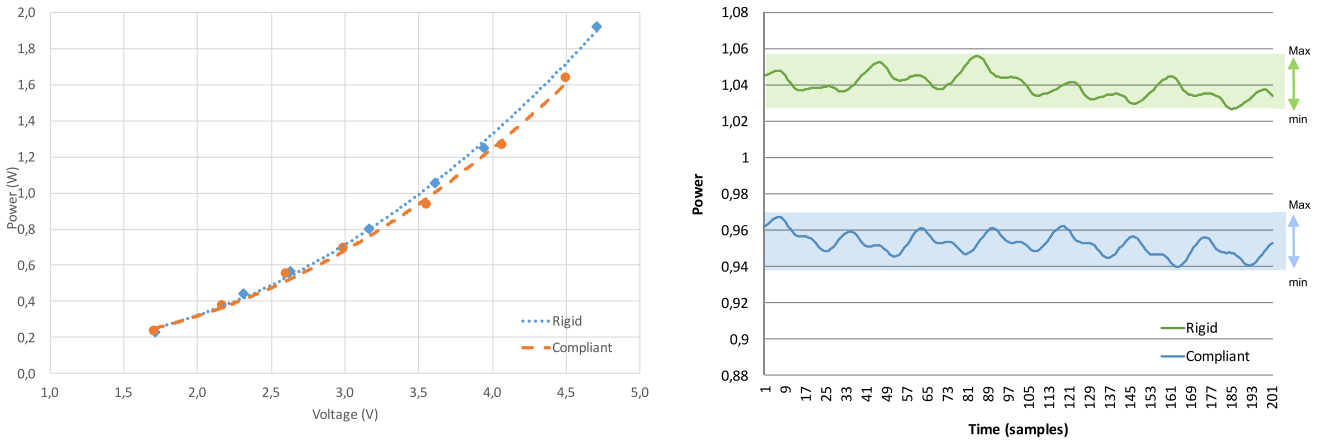

FIGURE 5. Left: Comparison of power consumption (measurements and fit models). Right: Comparison of peak power consumption (at ∼ 3.6 *V* input voltage).

where f_s is the sampling frequency (200 Hz) and f_c is the low-pass cutoff frequency, empirically set to 100 Hz.

B. RESULTS AND DISCUSSION

Figure 5 (left) shows the results of the measurements. As it can be noticed, the compliant mechanisms have a lower power consumption compared to the rigid mechanism. It also appears qualitatively that the power savings increase with the flapping frequency, which was an expected result. The numeric data are also reported in Table 2.

TABLE 2. Average power consumption.

Rigid			Compliant		
Voltage (V)	Current (A)	Power (W)	Voltage (V)	Current (A)	Power (W)
1.713	0,135	0.231	1.711	0,136	0.232
2.311	0,192	0.443	2.171	0,173	0.375
2.630	0,214	0.564	2.605	0,210	0.547
3.159	0,253	0.798	2.992	0,222	0.691
3.608	0,292	1.052	3.552	0,261	0.935
3.937	0,317	1.248	4.064	0,311	1.264
4.706	0,407	1.916	4.496	0,362	1.633

Figure 5 (left) also shows the trend lines that best fit the data. After an analysis of different alternatives we found that a polynomial line of order 2 was the best overall model that fit the data, both qualitatively and quantitatively: the coefficients of determination are $r^2 = 0.99$ in both cases. The equations of the curves are reported below.

$$Power_{Rigid}(v) = 0.1121\, v^2 - 0.1794\, v + 0.2152$$
$$Power_{Compliant}(v) = 0.1016 v^2 - 0.1449 v + 0.2028$$

where v is the input voltage. From these equation, we can compute the power saving. According to the models, saving of 4.3% are achieved at 4.5 V input voltage (corresponding approximately to 9 Hz flapping frequency). However, as mentioned earlier, the savings decrease for low flapping rates, and for input voltages lower than 2.87 V (flapping frequency of approximately 6 Hz) the rigid mechanism actually performed better than the compliant one.

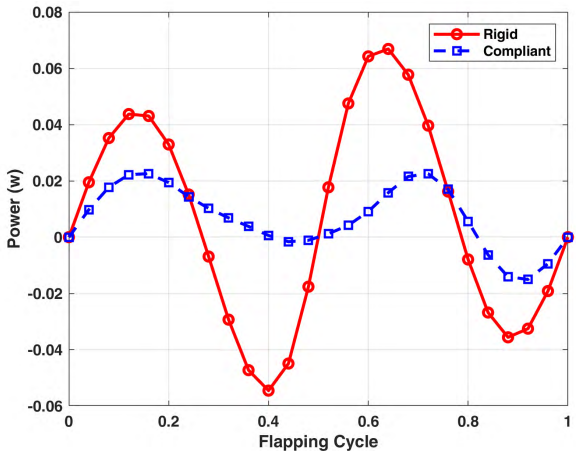

FIGURE 6. Theoretical power consumption predicted by the model.

The plots shown in Figure 5 (right) represent a zoom of the power consumption at 3.61*V* and 3.55 *V* input voltage (approximately 7 Hz flapping period) for the rigid and flexible mechanisms, respectively. As it can be observed, the peaks are bigger in plot of the rigid mechanism, which supports the claim that in addition to power saving, torque peaks are also reduced, as the mathematical analysis foresaw [33]. In this case, the difference between peaks is of 0.029 *W*in the case of the rigid prototype, and 0.022 *W* for the compliant one, which means a 25% reduction.

The main causes of deviation from the theoretical savings (up to 70%), we believe, are associated with friction at rotational joints, that in the in the theoretical framework are assumed to be negligible. However, in fact, the friction indeed exists in physical experiments. In addition, the rotational speed of the driving motor is supposed to be constant for simplicity in the prediction, but the motor speed varies

when aerodynamic loads act on wings. These adverse factors will result in the difference from the experimental results in power consumption. As shown in Fig. 5 (right), the variation trends on the measured power consumptions of both rigid and compliant mechanisms (see, e.g., sample intervals 26-55 and 55-84) are not strictly the same in every flapping cycle as the counterparts of the predicted ones due to the joint effects and other factors mentioned above. Finally, fabrication precision may be another cause for the gap. The assembly of the prototypes has been done manually, so even if all efforts have been made to guarantee a precise mounting, small deviations can be present. All such small approximations make the whole transmission mechanism not as optimal as designed, thereby leading to a generation of extra unwanted power consumption. Fig.6 shows an example of power consumption predicted by the theoretical model for the two mechanisms.

TABLE 3. Peak power reduction (see also Fig. 5, right.

Rigid		Compliant		
Voltage (V)	Max-min power (W)	Voltage (V)	Max-min power (W)	Saving
1.713	0.018	1.711	0.016	11.8%
2.630	0.024	2.605	0.022	6.2%
3.608	0,029	3.552	0,022	25.2%

Table 3 reports the same comparison for input voltages of $\sim$1.7 V and $\sim$ 2.6 V. In the remaining cases, a direct comparison is not representative due to the difference in input voltages between the rigid and compliant mechanisms.

V. CONCLUSIONS

In this paper, we have presented the design and testing of a transmission mechanism with compliant hinges for a flapping-wing micro air vehicle. The purpose of this mechanism is to minimize both peak and average input torque required by the motor during the flapping cycle.

A theoretical analysis of the input torque required by the motor has been carried out using two different methods, virtual work and rigid-body dynamics, that tackle the problem from the perspectives of work and energy, respectively. Compared to other optimization methods proposed in the literature, our methodology is suitable for pseudo-rigid models since internal interaction forces do not need to be considered. Furthermore, the elastic potential energy stored in the compliant joints can be easily taken into account.

The results of the experiments demonstrated that the compliant mechanism can significantly reduce both the average and the peak input torques. Therefore, we have demonstrated that the propose design allows energy saving, compared to classical rigid mechanisms and helps avoiding sharp shocks of the driving motor. The advantage of the compliant transmission mechanism is that allows adopting lighter structures at the benefit of payload and/or flight time, two critical issues in the field of FWMAVs.

Finally, we would like to point out that even though the methodology presented in this paper is applied to flapping transmission mechanisms, it can be generalized to the design of other compliant mechanisms. We believe that understanding energy-saving performance of biological systems will help developing light and energy-efficiency structures that can increase the performance of robotic systems (either *zoomorphic* or not) as far as autonomy and payload capabilities.

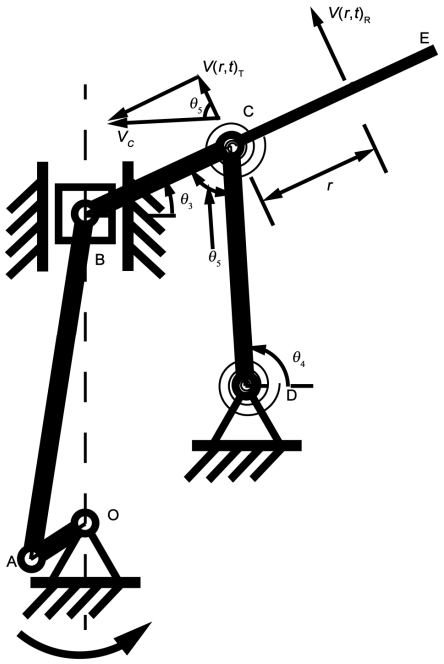

FIGURE 7. Sketch of the velocity analysis on the wing.

APPENDIX
AERODYNAMIC TORQUE CALCULATION

Aerodynamic torques generated by flapping wings play an important role in the flight stability of FWMAVs. In this section, we analyse the aerodynamic torque produced by wing motions in a cycle. To this purpose, an aerodynamic model based on the blade element theory [9] was employed. The following simplifying assumptions have been made:

- The irregular shape of a wing is approximated with a rectangle, whose length and width equal the length of the wing spar r_8 and the average wing chord c, respectively. The average chord c is computed according to wings' equivalent surface area.
- The wing is assumed to be rigid, i.e., without any twist and bend along the wing chord and the leading edge.
- The mass of the wing is considered to be negligible.

With these assumptions, the normal force produced by a single blade can be expressed according as follows:

$$dF_a = -\frac{1}{2}\rho C_1 |V(r,t)|^2 sgn(V(r,t))cdr, \qquad (26)$$

where $V(r,t)$ is a absolute velocity of an element, whose direction is contrary to the motion of the wing, ρ is the air density, 1.23 kg/m^3, and C_1 is the normal force coefficient of the blade [14].

Note that $V(r,t)$ consists of two parts: translational velocity $V(r,t)_T$ and rotational velocity of the wings $V(r,t)_R$ (see Fig. 7). Thus, $V(r,t) = V(r,t)_T + V(r,t)_R$ and $|V(r,t)| = |V(r,t)_T| + |V(r,t)_R|$.

Here, $|V(r,t)_T| = r_4\omega_4\, cos(\theta_5)$, $|V(r,t)_R| = r\omega_3$, and θ_5 is the intersection angle between the rocker r_3 and the thorax r_4 as shown in Fig. 7. Since the value of the translation velocity $V(r,t)_T$ is relatively small, its effect of wings' movements is also small. Therefore, $V(r,t)$ and $V(r,t)_R$ can be considered equal i.e., $V(r,t) = V(r,t)_R$. Also, $sgn(V(r,t)) = sgn(V(r,t)_R)$. Since $V(r,t)_R$ is positively proportional to ω_3, $sgn(V(r,t))$ can be described in terms of $sgn(\omega_3)$ as $sgn(V(r,t)) = sgn(\omega_3)$.

The instantaneous aerodynamic torque $d\tau_a$ can be expressed by the instantaneous force dF_a times the distance r along the wing spar,

$$d\tau_a = -\frac{1}{2}\rho C_1 r^3 \omega_3^2 sgn(\omega_3) c dr \tag{27}$$

From this equation, the total aerodynamic torque τ_a produced by the whole wing can be calculated.

REFERENCES

[1] R. M. Alexander and H. C. Bennet-Clark, "Storage of elastic strain energy in muscle and other tissues," *Nature*, vol. 265, no. 5590, pp. 114–117, 1977.
[2] M. Azhar, D. Campolo, G.-K. Lau, L. Hines, and M. Sitti, "Flapping wings via direct-driving by DC motors," in *Proc. IEEE Int. Conf. Robot. Autom. (ICRA)*, May 2013, pp. 1397–1402.
[3] S. S. Baek, K. Y. Ma, and R. S. Fearing, "Efficient resonant drive of flapping-wing robots," in *Proc. IEEE/RSJ Int. Conf. Intell. Robots Syst. (IROS)*, 2009, pp. 2854–2860.
[4] R. F. Chapman, *The Insects: Structure and Function*. Cambridge, U.K.: Cambridge Univ. Press, 1998.
[5] B. Cheng, X. Deng, and T. L. Hedrick, "The mechanics and control of pitching manoeuvres in a freely flying hawkmoth (Manduca sexta)," *J. Exp. Biol.*, vol. 214, no. 24, pp. 4092–4106, 2011.
[6] B. Cheng, J. A. Roll, and X. Deng, "Modeling and optimization of an electromagnetic actuator for flapping wing micro air vehicle," in *Proc. IEEE Int. Conf. Robot. Autom. (ICRA)*, May 2013, pp. 4035–4041.
[7] Y. W. Chin and G. K. Lau, "'Clicking' compliant mechanism for flapping-wing micro aerial vehicle," in *Proc. IEEE/RSJ Int. Conf. Intell. Robots Syst. (IROS)*, Oct. 2012, pp. 126–131.
[8] A. Cox, D. Monopoli, D. Cveticanin, M. Goldfarb, and E. Garcia, "The development of elastodynamic components for piezoelectrically actuated flapping micro-air vehicles," *J. Intell. Mater. Syst. Struct.*, vol. 13, no. 9, pp. 611–615, 2002.
[9] C. P. Ellington, "The aerodynamics of insect flight. I. The quasi-steady analysis," *Philos. Trans. Roy. Soc. B, Biol. Sci.*, vol. 305, no. 1122, pp. 1–15, 1984.
[10] C. P. Ellington, "Power and efficiency of insect flight muscle," *J. Exp. Biol.*, vol. 115, no. 1, pp. 293–304, 1985.
[11] T. L. Hedrick, B. Cheng, and X. Deng, "Wingbeat time and the scaling of passive rotational damping in flapping flight," *Science*, vol. 324, no. 5924, pp. 252–255, 2009.
[12] L. Hines, D. Campolo, and M. Sitti, "Liftoff of a motor-driven, flapping-wing microaerial vehicle capable of resonance," *IEEE Trans. Robot.*, vol. 30, no. 1, pp. 220–232, Feb. 2014.
[13] L. L. Howell, *Compliant Mechanisms*. Hoboken, NJ, USA: Wiley, 2001.
[14] Z. A. Khan and S. K. Agrawal, "Design of flapping mechanisms based on transverse bending phenomena in insects," in *Proc. IEEE Int. Conf. Robot. Autom. (ICRA)*, May 2006, pp. 2323–2328.
[15] G.-K. Lau, Y.-W. Chin, J. T.-W. Goh, and R. J. Wood, "Dipteran-insect-inspired thoracic mechanism with nonlinear stiffness to save inertial power of flapping-wing flight," *IEEE Trans. Robot.*, vol. 30, no. 5, pp. 1187–1197, Oct. 2014.
[16] R. Madangopal, Z. A. Khan, and S. K. Agrawal, "Biologically inspired design of small flapping wing air vehicles using four-bar mechanisms and quasi-steady aerodynamics," *J. Mech. Des.*, vol. 127, no. 4, pp. 809–816, 2005.
[17] J. A. Roll, B. Cheng, and X. Deng, "Design, fabrication, and experiments of an electromagnetic actuator for flapping wing micro air vehicles," in *Proc. IEEE Int. Conf. Robot. Autom. (ICRA)*, May 2013, pp. 809–815.
[18] J. A. Roll, B. Cheng, and X. Deng, "An electromagnetic actuator for high-frequency flapping-wing microair vehicles," *IEEE Trans. Robot.*, vol. 31, no. 2, pp. 400–414, Apr. 2015.
[19] M. Ryan and H.-J. Su, "Classification of flapping wing mechanisms for micro air vehicles," in *Proc. Int. Design Eng. Tech. Conf. Comput. Inf. Eng. Conf.*, 2012, pp. 105–115.
[20] R. Sahai, K. C. Galloway, and R. J. Wood, "Elastic element integration for improved flapping-wing micro air vehicle performance," *IEEE Trans. Robot.*, vol. 29, no. 1, pp. 32–41, Feb. 2013.
[21] M. Sitti, "Piezoelectrically actuated four-bar mechanism with two flexible links for micromechanical flying insect thorax," *IEEE/ASME Trans. Mechatronics*, vol. 8, no. 1, pp. 26–36, Mar. 2003.
[22] R. E. Snodgrass, *Principles of Insect Morphology*. Ithaca, NY, USA: Cornell Univ. Press, 1935.
[23] T. Tantanawat and S. Kota, "Design of compliant mechanisms for minimizing input power in dynamic applications," *J. Mech. Des.*, vol. 129, no. 10, pp. 1064–1075, 2007.
[24] Z. E. Teoh, S. B. Fuller, P. Chirarattananon, N. Prez-Arancibia, J. D. Greenberg, and R. J. Wood, "A hovering flapping-wing microrobot with altitude control and passive upright stability," in *Proc. IEEE/RSJ Int. Conf. Intell. Robots Syst. (IROS)*, Oct. 2012, pp. 3209–3216.
[25] Y. Wang and Z. Cai, "A hybrid multi-swarm particle swarm optimization to solve constrained optimization problems," *Frontiers Comput. Sci. China*, vol. 3, no. 1, pp. 38–52, 2009.
[26] T. Weis-Fogh, "Energetics of hovering flight in hummingbirds and in Drosophila," *J. Exp. Biol.*, vol. 56, no. 1, pp. 79–104, 1972.
[27] T. Weis-Fogh, "Quick estimates of flight fitness in hovering animals, including novel mechanisms for lift production," *J. Exp. Biol.*, vol. 59, no. 1, pp. 169–230, 1973.
[28] R. J. Wood, "Liftoff of a 60 mg flapping-wing MAV," in *Proc. IEEE/RSJ Int. Conf. Intell. Robots Syst. (IROS)*, Oct. 2007, pp. 1889–1894.
[29] R. J. Wood, "The first takeoff of a biologically inspired at-scale robotic insect," *IEEE Trans. Robot.*, vol. 24, no. 2, pp. 341–347, Apr. 2008.
[30] R. J. Wood, E. Steltz, and R. S. Fearing, "Optimal energy density piezoelectric bending actuators," *Sens. Actuators A, Phys.*, vol. 119, no. 2, pp. 476–488, 2005.
[31] Y.-Q. Yu, L. L. Howell, C. Lusk, Y. Yue, and M. G. He, "Dynamic modeling of compliant mechanisms based on the pseudo-rigid-body model," *J. Mech. Des.*, vol. 127, no. 4, pp. 760–765, 2005.
[32] C. Zhang and C. Rossi, "A review of compliant transmission mechanisms for bio-inspired flapping-wing micro air vehicles," *Bioinspiration Biomimetics*, vol. 12, no. 12, p. 025005, 2017.
[33] C. Zhang, C. Rossi, W. He, and J. Colorado, "Virtual-work-based optimization design on compliant transmission mechanism for flapping-wing aerial vehicles," in *Proc. Int. Conf. Manipulation, Autom. Robot. Small Scales (MARSS)*, Jul. 2016, pp. 1–6.

CHAO ZHANG received the B.Sc. and M.Sc. degrees from Northwestern Polytechnical University, Xi'an, China, in 2010 and 2013, respectively, and the Ph.D. degree in automatic control and robotics from the Universidad Politécnica de Madrid, Spain, in 2016. He is currently holding the Postdoctoral position with the Department of Automation, Shanghai Jiao Tong University, Shanghai, China. His research interests include kinematics and dynamics of robots, flapping-wing MAVs, compliant mechanisms and optimization design, flight control, and fuzzy neural networks.

CLAUDIO ROSSI received the Ph.D. degree in computer science from the University of Bologna, Italy, in 2001. He has been a Visiting Researcher with the Leiden Institute of Advanced Computer Science, NL, a Postdoctoral Fellow with the Department of Artificial Intelligence, Universidad Politécnica de Madrid (UPM), and a Visiting Professor with the University Carlos III of Madrid. From 2005 to 2009, he was the ''Ramon y Cajal'' Research Fellow with UPM, and since 2009, he has been a Professor with UPM. He has participated in several international research projects, and he has published around 80 papers in scientific journals and international conferences, on the topics of artificial intelligence, robotics, and biomimetics. His research interests, initially centered on nature-inspired search techniques for hard optimization problems, have been later directed towards applications of artificial intelligence to robotics. Since 2009, his research interests have been directed towards and bio-inspired systems, shifting form nature-based (software) search techniques to nature-based physical systems.